Green Chemistry

ROYAL SOCIETY OF CHEMISTRY

COMMUNICATION

View Article Online
View Journal | View Issue

Cite this: *Green Chem.*, 2023, **25**, 6207

Received 4th May 2023,
Accepted 18th July 2023

DOI: 10.1039/d3gc01461d

rsc.li/greenchem

Designing dual-atom cobalt catalysts anchored on amino-functionalized MOFs for efficient CO_2 photoreduction†

Meng-Ting Ming,‡ Yu-Chen Wang,‡ Wei-Xue Tao, Wen-Jie Shi, * Di-Chang Zhong* and Tong-Bu Lu *

Unlocking the potential of sustainable fuel production through the development of highly efficient CO_2 reduction catalysts under visible light irradiation remains an ongoing challenge. Herein, we report a strategically designed Zr-based metal–organic framework (MOF) photocatalyst, incorporating binuclear cobalt complexes as catalytic sites for effective CO_2 reduction. Impressively, our Co_2-MOF(–NH_2) catalyst showcased a CO yield of 2.44 mmol g_{Co}^{-1} h^{-1}, outperforming its mononuclear counterpart Co-MOF(–NH_2) (0.23 mmol g_{Co}^{-1} h^{-1}) by 10.5 times, underscoring the exceptional catalytic capabilities of the dual-atom catalyst. A combination of experimental findings and Density Functional Theory (DFT) calculations unveiled the synergistic catalytic effect between the two Co sites and the heightened light absorption attributed to the incorporation of the amino group. Notably, such characteristics are evocative of cooperative catalysis observed in biological enzyme systems. This study highlights a pioneering, bioinspired approach to designing efficient dual-atom MOF photocatalysts for CO_2 reduction, offering significant implications for the future of sustainable energy production.

Artificial photosynthesis, which converts sunlight-driven CO_2 into valuable chemicals and fuels, has garnered significant attention as a sustainable means of solar energy conversion and storage.[1–3] Metal–organic frameworks (MOFs),[4,5] characterized by their high surface area,[6] tunable pore size,[7] and customizable chemistry,[8–10] have emerged as promising platforms for photocatalysis.[11–17] Anchoring atomic-level catalysts onto MOFs has been widely explored to enhance their catalytic performance in CO_2 reduction reactions (CO_2RR),[18] particularly for single-atom catalysts.[19–21] Nevertheless, research on MOF-anchored dual-atom catalysts and the synergistic effect of two adjacent atoms within MOFs remains limited.[22–25]

In the realm of biological catalysis, dual-atom catalytic sites have demonstrated exceptional performance,[26,27] indicating their potential for designing efficient catalysts.[28–30] Inspired by these biological systems, we sought to develop a MOF-based dual-atom cobalt catalyst to explore the potential benefits of such a design for CO_2RR.[31] Our previous work on molecular binuclear complexes as photocatalysts for CO_2RR revealed that the synergistic effect between two Co sites could significantly enhance catalytic performance compared to mononuclear counterparts.[32] To further delve into the significance of binuclear metal synergistic catalysis, we synthesized a binuclear heterometallic complex, which displayed a great catalytic activity.[33]

Capitalizing on these findings, we integrated a highly active binuclear cobalt complex into an amino-functionalized MOF, thereby creating a synergistic dual-atom catalyst (Scheme 1). Remarkably, our newly developed MOF-based binuclear catalyst [Co_2-MOF(–NH_2)] demonstrated exceptional catalytic

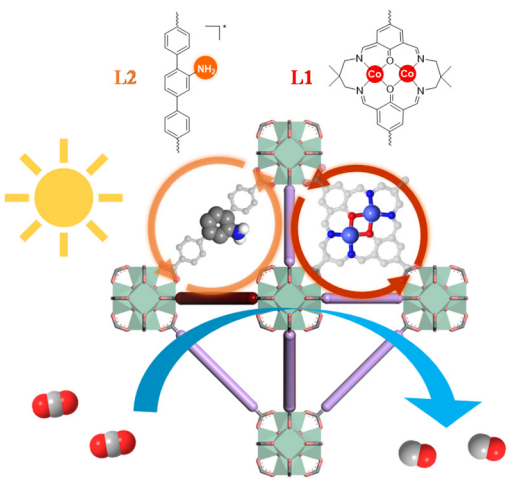

Scheme 1 Framework structures and bridging ligands of Co_2-MOF (–NH_2).

MOE International Joint Laboratory of Materials Microstructure, Institute for New Energy Materials & Low Carbon Technologies, School of Material Science & Engineering, Tianjin University of Technology, Tianjin 300384, China.
E-mail: wjshi@email.tjut.edu.cn, dczhong@email.tjut.edu.cn, lutongbu@tjut.edu.cn

†Electronic supplementary information (ESI) available: The syntheses and characterization of the catalyst, DFT calculation, supplementary figures and tables. See DOI: https://doi.org/10.1039/d3gc01461d

‡These two authors contributed equally to this paper.

activity for CO_2RR, with a CO yield of 2.44 mmol g_{Co}^{-1} h^{-1}, a 10.5-fold increase compared to its mononuclear counterpart, Co-MOF(–NH_2). The enhanced catalytic capacity is attributable to the synergistic catalysis effect of the binuclear Co sites, corroborated by experimental evidence and DFT calculations.

This study highlights the potential of MOF-based binuclear catalysts for augmenting the catalytic performance of CO_2RR and contributes to the growing body of research on MOF-anchored dual-atom catalysts. Our findings pave the way for designing highly efficient CO_2 reduction catalysts harnessing synergistic metal sites within MOFs, offering new opportunities for sustainable energy production and storage.

The binuclear cobalt complex, $\{Co_2(CH_3)_2C[CH_2N{=}CH(1\text{-}COOH\text{-}4\text{-}OH\text{-}3,5\text{-}C_6H_3)CH{=}NCH_2]_2C(CH_3)_2\}(ClO_4)_2$ (L1) was prepared according to previously reported literatures (Schemes S1–2 and Fig. S1–4†).[34,35] Then Co$_2$-MOF(–NH_2) was synthesized by a solvothermal reaction of $ZrCl_4$, L1 and 2′-amino-[1,1′:4′,1″-terphenyl]-4,4″-dicarboxylic acid (L2) in DMF with acetic acid at 120 °C.[36,37] L-MOF(–NH_2) and Co$_2$-MOF use the same method, with the exception of changing L1 to L4 (a complex with similar structure of L1 without Co site, as shown in Scheme S2†), or L2 to [1,1′:4′,1″-terphenyl]-4,4″-dicarboxylic acid (L3), respectively (Schemes S3 and 4†). Co-MOF(–NH_2) was prepared by the reaction of L-MOF(–NH_2) and Co $(ClO_4)_2{\cdot}6H_2O$. As shown in Fig. 1a, the powder X-ray diffraction (PXRD) patterns of the four MOFs all closely match the simulated one of UiO-68,[38] indicating that the framework keeps stable after introducing ligand L1 or L4. High-resolution transmission electron microscopy (HRTEM) images and elemental mapping illustrated the octahedral morphologies of Co$_2$-MOF (–NH_2) with homogeneous distribution of Co and Zr (Fig. 1b–d). The size of Co$_2$-MOF(–NH_2), Co-MOF(–NH_2), L-MOF(–NH_2) and Co$_2$-MOF was measured to be 2.6 μm, 1.5 μm, 1.6 μm and 3.1 μm, respectively (Fig. S5†). Fourier transform infrared spectra (FT-IR) further confirmed the isostructural of these MOFs, with minor variances due to material sizes and metal center coordination (Fig. S6†). Co$_2$-MOF(–NH_2) showed good stability (Fig. S7†).

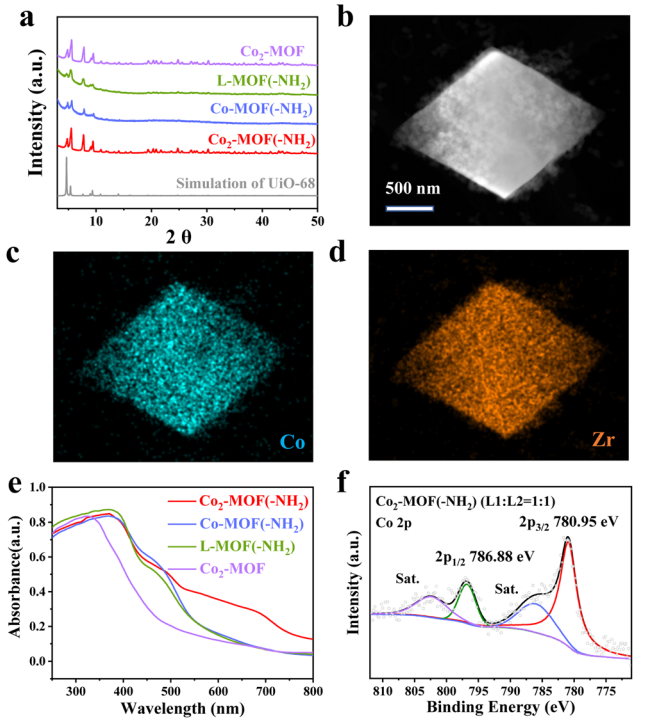

Fig. 1 (a) PXRD patterns of Co$_2$-MOF(–NH_2) (red), Co-MOF(–NH_2) (blue), L-MOF(–NH_2) (green) and Co$_2$-MOF (purple). (b) HRTEM image and (c–d) EDS elemental mapping for Co and Zr of Co$_2$-MOF(–NH_2). (e) UV-Vis DRS of Co$_2$-MOF(–NH_2) (red), Co-MOF(–NH_2) (blue), L-MOF (–NH_2) (green) and Co$_2$-MOF (purple). (f) XPS profiles of Co 2p for Co$_2$-MOF(–NH_2) (L1 : L2 = 1 : 1).

Using UV-Vis DRS (Fig. 1e and S8†), we observed an extension in light absorption from 480 nm to 800 nm in amino functional catalysts following the introduction of amino group. The steady-state photoluminescence (PL) spectra of L1 and L2 were also depicted in Fig. S9.† The high-resolution X-ray photoelectron spectroscopy (XPS) of Co 2p for Co$_2$-MOF(–NH_2) (L1 : L2 = 1 : 1) exhibited the main peaks of Co $2p_{3/2}$ and Co $2p_{1/2}$ at 780.95 and 796.88 eV, respectively, indicating that the valence of Co was +2 (Fig. 1f).[39] However, there was no obvious Co species can be detected by XPS in Co$_2$-MOF(–NH_2) (L1 : L2 = 1 : 5), Co-MOF(–NH_2) and Co$_2$-MOF due to the low Co content beyond the detection limit (Fig. S10†). In addition, Co$_2$-MOF (–NH_2) possesses higher CO_2 adsorption capacity than the others, with an adsorption amount of 24.2 cm^3 g^{-1} at 1 atm (Fig. S11†), which might result in enhanced catalytic performance of CO_2RR.[40]

Based on the characterization results presented above, the CO_2 reduction reactions were conducted in a CO_2-saturated mixture of 5 mL CH_3CN and H_2O (v/v = 4/1) along with MOFs as photocatalysts. A sacrificial reductant in the form of 1,3-dimethyl-2-phenyl-2,3-dihydro-1*H*-benzoimidazole (BIH) was also employed. In order to figure the best ratio of L1 and L2, a series of Co$_2$-MOFs(–NH_2) with different molar ratios of L1 and L2, ranging from 1 : 1 to 1 : 20, were synthesized and employed as photocatalysts of CO_2RR. The PXRD pattern exhibited insignificant differences amongst the five materials (Fig. S12a†). The consumption of the chemicals and the contents of Co and Zr were shown in Tables S1, S2 and S3,† respectively. As shown in Fig. S12b,† the highest CO yield was obtained with the *n* (L1) : *n* (L2) ratio of 1 : 5 (37.85 μmol g^{-1} h^{-1}), which is 3.64, 2.68, 1.48, 2.10 times that of Co$_2$-MOFs(–NH_2) with the *n* (L1) : *n* (L2) ratio of 1 : 20, 1 : 10, 1 : 2 and 1 : 1, respectively. It was hypothesized that inadequate active sites hindered the catalytic activity when the ratio of *n* (L1) : *n* (L2) was below 1 : 5, while beyond this ratio, the lack of photosensitive molecules (L2) obstructed the light absorption of Co$_2$-MOFs(–NH_2). As a result, the 1 : 5 molar ratios of L1 and L2 in Co$_2$-MOFs(–NH_2) was chosen as the model catalyst to investigate the CO_2 photoreduction.

Fig. 2a and b depict the CO production rate of Co$_2$-MOF (–NH_2), Co-MOF(–NH_2), L-MOF(–NH_2) and Co$_2$-MOF were 37.85, 2.05, 0.00 and 5.41 μmol g^{-1} h^{-1}, respectively, with trace H_2 detected (Fig. S13†). These findings suggest that the Co

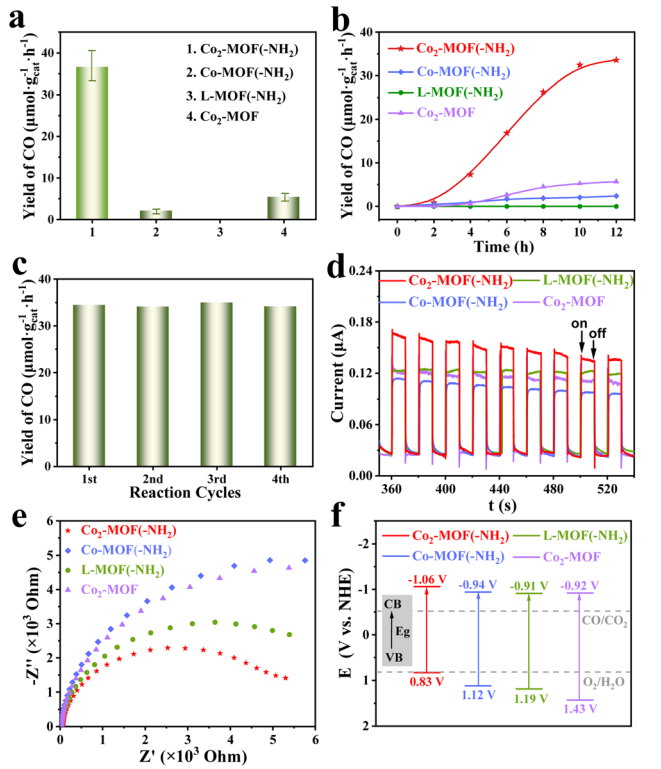

Fig. 2 (a) Comparison of CO production rate of Co_2-MOF(–NH_2), Co-MOF(–NH_2), L-MOF(–NH_2) and Co_2-MOF. (c) CO yields of Co_2-MOF (–NH_2) for 4 reaction cycles. (b) Time-resolved CO productions, (d) photocurrent tests, (e) EIS plots and (f) band gap diagram of Co_2-MOF (–NH_2) (red), Co-MOF(–NH_2) (blue), L-MOF(–NH_2) (green) and Co_2-MOF (purple).

sites are the active centers and the amino functional ligand improves the CO_2RR activity of the MOF-based catalyst. CO yield *versus* Co content of Co_2-MOF(–NH_2) (2.44 mmol g_{Co}^{-1} h^{-1}) was 10.48 times as high as Co-MOF(–NH_2) (0.23 mmol g_{Co}^{-1} h^{-1}) owing to the synergistic catalysis effect, and trace amounts of CO were produced in homogenous system of L1 (Fig. S14†). Furthermore, it was observed that the absence of catalyst, BIH, light or CO_2 gas led to no CO production, indicating that all those components are crucial in the reaction system (Fig. S15a†). Photocatalytic reactions were performed using ^{13}C labeled CO_2, and the peak of m/z = 29 was observed, confirming that CO was generated from the reduction of CO_2 (Fig. S15b†). No liquid product was detected by ion chromatography (IC). Compare to recently reported MOF-based catalysts, Co_2-MOF(–NH_2) exhibited a good performance in photocatalytic CO_2 reduction (Table S4†). Later, the durability of Co_2-MOF(–NH_2) was investigated, and it was found that the CO yields remained steady in four runs (Fig. 2c). The PXRD pattern and SEM images of the recycled Co_2-MOF(–NH_2) were consistent with the pristine one (Fig. S16†), demonstrating the well-maintained integrity and crystallinity.

To elucidate the incremental photocatalytic activity of Co_2-MOF(–NH_2), photocurrent and EIS measurement were carried out. As shown in Fig. 2d and e, Co_2-MOF(–NH_2) exhibited significantly enhanced photocurrent response and the smallest impedance radius, standing for superior charge separation and transfer efficiency. Moreover, Tauc plots showed that the band gap energies of Co_2-MOF(–NH_2), Co-MOF(–NH_2), L-MOF (–NH_2) and Co_2-MOF as 1.89, 2.06, 2.10 and 2.35 eV, respectively. Mott–Schottky measurement showed the flat bands of Co_2-MOF(–NH_2), Co-MOF(–NH_2), L-MOF(–NH_2), and Co_2-MOF calculated to be −1.06, −0.94, −0.91 and −0.92 V, respectively (Fig. S17†). The corresponding band gap diagram is presented in Fig. 2f. As their CB potentials are more negative than the redox potential of photocatalytic CO_2 reduction to CO (−0.52 V *vs.* NHE), all catalysts meet the thermodynamic prerequisites for this transformation.

To further reveal the catalytic mechanism of Co_2-MOF (–NH_2), fluorescence quenching experiment of L2 was conducted with excitation at 360 nm. As shown in Fig. S18a,† an emission peak corresponding to excited [L2]* appeared at 409 nm, which reduced clearly with the addition of L1. In contrast, the fluorescence intensity showed very limited decrease when BIH was added (Fig. S18c†). The results above elucidate that the L2 parts in Co_2-MOF(–NH_2) was quenched by L1 parts through oxidative quenching pathway.[41] Moreover, the fluorescence quenching intensity is linearly related to the concentration of L1 or BIH, demonstrates the diffusion-controlled electron transfer process (Fig. S18b and d†).[32,33]

In addition, *in situ* FTIR measurements and DFT calculations were carried out to evaluate the reaction processes and related active species. As shown in Fig. 3a, two evident peaks of *COOH (1637 cm^{-1}) and *CO (2077 cm^{-1}) intermediates (* means the adsorption site) can be detected, demonstrating that the formation of *CO was the rate-determining step.[42] Co-MOF(–NH_2) displayed the similar results (Fig. S19†). It has been further revealed by DFT calculations of energy barriers. As shown in Fig. 3b and c, the Co center in catalyst (Cat) accepted an electron from –NH_2 to afford the Int-1 firstly.[43] Then Int-1 adsorbed a CO_2 to form Co–CO_2 adduct (Int-2) with the free-energy change (ΔG) of 0.10 eV. The Int-2 undergoes a proton-coupled electron transfer (PCET) process to generate Int-3. The ΔG of this PCET process (0.50 eV) is lower than the

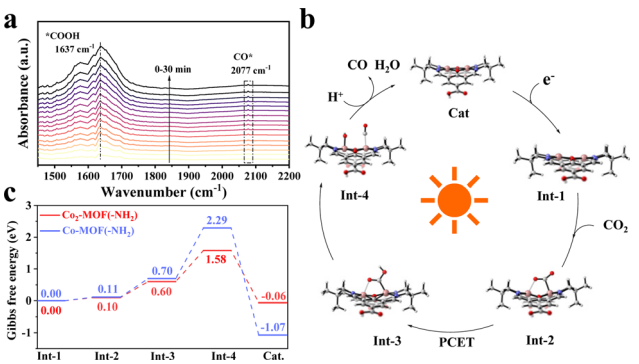

Fig. 3 (a) *In situ* FTIR spectra, (b) Proposed catalytic cycle for the photocatalytic CO_2RR catalyzed by Co_2-MOF(–NH_2) and (c) DFT calculations of energy barriers.

formation of Int-4 (0.98 eV). After adding a proton (H^+) to form a water molecule, CO was released and the Cat regenerated through an exothermal process (−1.64 eV).[44,45] The rate-determining step ΔG value on Co-MOF(–NH_2) (1.59 eV) is much higher than on Co_2-MOF(–NH_2), the projected density of states (PDOS) analysis suggests that the binuclear Co introduction modulates the Co 3d orbital of. The d-band center shifts from −1.3 eV in Co-MOF(–NH_2) to −1.5 eV in Co_2-MOF(–NH_2), demonstrating stronger COOH* adsorption on Co_2 site (Fig. S20†),[46] which can be attributed to the binuclear metal synergistic catalysis effect of Co_2-MOF(–NH_2).

In summary, we synthesized a binuclear cobalt complex, based on which three Zr-based MOFs were fabricated and applied to photocatalytic CO_2RR. The integration of L1 and L2 in MOFs dramatically boosted the photo-catalytic CO_2-to-CO conversion without any additional photosensitizer. Photo- and electro-chemical measurements and DFT calculation indicated that the incremental catalytic activities of Co_2-MOF(–NH_2) is likely attribute to the increased visible-light absorption and charge separation. Fluorescence testing revealed an oxidative quenching pathway in which the photoexcited [L2]* inject electrons to the catalytic sites to impulse CO_2RR. This work provides a new idea for improving the catalytic performance of MOF-based photocatalyst without the usage of precious metal photosensitizer.

Conflicts of interest

There are no conflicts to declare.

Acknowledgements

This work was supported by the National Key R&D Program of China (2022YFA1502902), the National Natural Science Foundation of China (22271218, 22071182, 22201209, and 21931007).

References

1 M. N. Dods, S. C. Weston and J. R. Long, *Adv. Mater.*, 2022, **34**, 2204277.
2 E. Gong, S. Ali, C. B. Hiragond, H. S. Kim, N. S. Powar, D. Kim, H. Kim and S.-I. In, *Energy Environ. Sci.*, 2022, **15**, 880–937.
3 X. Deng, R. Long, C. Gao and Y. J. Xiong, *Curr. Opin. Electrochem.*, 2019, **17**, 114–120.
4 O. M. Yaghi, G. M. Li and H. L. Li, *Nature*, 1995, **378**, 703–706.
5 H. L. Li, M. Eddaoudi, M. O'Keeffe and O. M. Yaghi, *Nature*, 1999, **402**, 276–279.
6 H. Furukawa, K. E. Cordova, M. O'Keeffe and O. M. Yaghi, *Science*, 2013, **341**, 1230444.
7 D. D. Li, H. Q. Xu, L. Jiao and H. L. Jiang, *EnergyChem*, 2019, **1**, 100005.
8 H. X. Deng, C. J. Doonan, H. Furukawa, R. B. Ferreira, J. Towne, C. B. Knobler, B. Wang and O. M. Yaghi, *Science*, 2010, **327**, 846–850.
9 Y. P. Wei, Y. Liu, F. Guo, X. Y. Dao and W. Y. Sun, *Dalton Trans.*, 2019, **48**, 8221–8226.
10 A. A. Zhang, R. Wang, H. B. Huang, T. F. Liu and R. Cao, *Chin. Chem. Lett.*, 2023, **34**, 107311.
11 Y. Song, Y. H. Pi, X. Y. Feng, K. Y. Ni, Z. W. Xu, J. S. Chen, Z. Li and W. B. Lin, *J. Am. Chem. Soc.*, 2020, **142**, 6866–6871.
12 T. C. Zhuo, Y. Song, G. L. Zhuang, L. P. Chang, S. Yao, W. Zhang, Y. Wang, P. Wang, W. B. Lin, T. B. Lu and Z. M. Zhang, *J. Am. Chem. Soc.*, 2021, **143**, 6114–6122.
13 H. Takezawa and M. Fujita, *Bull. Chem. Soc. Jpn.*, 2021, **94**, 2351–2369.
14 P. M. Stanley, J. Haimerl, N. B. Shustova, R. A. Fischer and J. Warnan, *Nat. Chem.*, 2022, **14**, 1342–1356.
15 T. Wang, L. Zhang, J. Liu, X. X. Li, L. Yuan, S. L. Li and Y. Q. Lan, *Chem. Commun.*, 2022, **58**, 7507–7510.
16 P. M. Stanley, A. Y. Su, V. Ramm, P. Fink, C. Kimna, O. Lieleg, M. Elsner, J. A. Lercher, B. Rieger, J. Warnan and R. A. Fischer, *Adv. Mater.*, 2023, **35**, 2207380.
17 K. Sun, Y. Y. Qian and H. L. Jiang, *Angew. Chem., Int. Ed.*, 2023, **62**, e202217565.
18 L. Z. Zeng, Y. H. Cao, Z. Li, Y. H. Dai, Y. K. Wang, B. An, J. Z. Zhang, H. Li, Y. Zhou, W. B. Lin and C. Wang, *ACS Catal.*, 2021, **11**, 11696–11705.
19 H. B. Zhang, J. Wei, J. C. Dong, G. G. Liu, L. Shi, P. F. An, G. X. Zhao, J. T. Kong, X. J. Wang, X. G. Meng, J. Zhang and J. H. Ye, *Angew. Chem., Int. Ed.*, 2016, **55**, 14310–14314.
20 D. C. Liu, T. Ouyang, R. Xiao, W. J. Liu, D. C. Zhong, Z. T. Xu and T. B. Lu, *ChemSusChem*, 2019, **12**, 2166–2170.
21 X. L. Zu, Y. Zhao, X. D. Li, R. H. Chen, W. W. Shao, L. Li, P. Z. Qiao, W. S. Yan, Y. Pan, Q. Xu, J. F. Zhu, Y. F. Sun and Y. Xie, *Angew. Chem., Int. Ed.*, 2023, **62**, e202215247.
22 C. C. Hou, H. F. Wang, C. X. Li and Q. Xu, *Energy Environ. Sci.*, 2020, **13**, 1658–1693.
23 L. Jiao, J. T. Zhu, Y. Zhang, W. J. Yang, S. Y. Zhou, A. W. Li, C. F. Xie, X. S. Zheng, W. Zhou, S. H. Yu and H. L. Jiang, *J. Am. Chem. Soc.*, 2021, **143**, 19417–19424.
24 L. Jiao and H. L. Jiang, *Chin. J. Catal.*, 2023, **45**, 1–5.
25 J. D. Xiao, R. Li and H. L. Jiang, *Small Methods*, 2023, **7**, 2201258.
26 A. Kumar, V. Hasija, A. Sudhaik, P. Raizada, Q. Van Le, P. Singh, T.-H. Pham, T. Kim, S. Ghotekar and V.-H. Nguyen, *Chem. Eng. J.*, 2022, **430**, 133031.
27 C. J. Zhang, P. Gotico, R. Guillot, D. Dragoe, W. Leibl, Z. Halime and A. Aukauloo, *Angew. Chem., Int. Ed.*, 2023, **62**, e202214665.
28 X. Han and S. H. Yang, *Chem*, 2022, **8**, 2584–2586.
29 H. M. Liu, H. P. Rong and J. T. Zhang, *ChemSusChem*, 2022, **15**, e202200498.
30 J. Li, H. L. Huang, W. J. Xue, K. Sun, X. H. Song, C. R. Wu, L. Nie, Y. Li, C. Y. Liu, Y. Pan, H. L. Jiang, D. Mei and C. L. Zhong, *Nat. Catal.*, 2021, **4**, 719–729.

31 L. Lin, H. B. Li, C. C. Yan, H. F. Li, R. Si, M. R. Li, J. P. Xiao, G. X. Wang and X. H. Bao, *Adv. Mater.*, 2019, **31**, 1903470.
32 T. Ouyang, H. H. Huang, J. W. Wang, D. C. Zhong and T. B. Lu, *Angew. Chem., Int. Ed.*, 2017, **56**, 738–743.
33 T. Ouyang, H. J. Wang, H. H. Huang, J. W. Wang, S. Guo, W. J. Liu, D. C. Zhong and T. B. Lu, *Angew. Chem., Int. Ed.*, 2018, **57**, 16480–16485.
34 M. Zhou, Z. F. Ju and D. Q. Yuan, *Chem. Commun.*, 2018, **54**, 2998–3001.
35 S. Pappuru, K. B. Idrees, Z. Chen, D. Shpasser and O. M. Gazit, *Dalton Trans.*, 2021, **50**, 6631–6636.
36 W. Morris, B. Volosskiy, S. Demir, F. Gándara, P. L. McGrier, H. Furukawa, D. Cascio, J. F. Stoddart and O. M. Yaghi, *Inorg. Chem.*, 2012, **51**, 6443–6445.
37 Y. A. Li, S. Yang, Q. Y. Li, J. P. Ma, S. J. Zhang and Y. B. Dong, *Inorg. Chem.*, 2017, **56**, 13241–13248.
38 P. M. Stanley, J. Haimerl, C. Thomas, A. Urstoeger, M. Schuster, N. B. Shustova, A. Casini, B. Rieger, J. Warnan and R. A. Fischer, *Angew. Chem., Int. Ed.*, 2021, **60**, 17854–17860.
39 Y. N. Gong, B. Z. Shao, J. H. Mei, W. Yang, D. C. Zhong and T. B. Lu, *Nano Res.*, 2022, **15**, 551–556.
40 Y. Y. Liu, Y. M. Yang, Q. L. Sun, Z. Y. Wang, B. B. Huang, Y. Dai, X. Y. Qin and X. Y. Zhang, *ACS Appl. Mater. Interfaces*, 2013, **5**, 7654–7658.
41 W. Yang, H. J. Wang, R. R. Liu, J. W. Wang, C. Zhang, C. Li, D. C. Zhong and T. B. Lu, *Angew. Chem., Int. Ed.*, 2021, **60**, 409–414.
42 N.-Y. Huang, H. He, S. Liu, H.-L. Zhu, Y.-J. Li, J. Xu, J.-R. Huang, X. Wang, P.-Q. Liao and X.-M. Chen, *J. Am. Chem. Soc.*, 2021, **143**, 17424–17430.
43 D. R. Sun, Y. H. Fu, W. J. Liu, L. Ye, D. K. Wang, L. Yang, X. Z. Fu and Z. H. Li, *Chem. – Eur. J.*, 2013, **19**, 14279–14285.
44 D. C. Grills, M. Z. Ertem, M. McKinnon, K. T. Ngo and J. Rochford, *Coord. Chem. Rev.*, 2018, **374**, 173–217.
45 J. H. Zhang, D. C. Zhong and T. B. Lu, *Acta Phys.-Chim. Sin.*, 2021, **37**, 2008068.
46 F. T. Zhang, P. Wang, R. Y. Zhao, Y. D. Wang, J. J. Wang, B. X. Han and Z. M. Liu, *ChemSusChem*, 2022, **15**, e202201267.